Monthly Notices
of the
ROYAL ASTRONOMICAL SOCIETY

MNRAS **489,** L53–L57 (2019)
Advance Access publication 2019 August 12

doi:10.1093/mnrasl/slz126

Evidence for C II diffuse line emission at redshift $z \sim 2.6$

Shengqi Yang,[1]★ Anthony R. Pullen[1] and Eric R. Switzer[2]

[1]*Center for Cosmology and Particle Physics, Department of Physics, New York University, 726 Broadway, New York, NY 10003, USA*
[2]*NASA Goddard Space Flight Center, Greenbelt, MD 20771, USA*

Accepted 2019 July 5. Received 2019 July 3; in original form 2019 March 21

ABSTRACT

C II is one of the brightest emission lines from star-forming galaxies and is an excellent tracer for star formation. Recent work measured the C II emission line amplitude for redshifts $2 < z < 3.2$ by cross-correlating Planck High Frequency Instrument emission maps with tracers of overdensity from the Baryon Oscillation Spectroscopic Sky Survey, finding $I_{\rm C\,II} = 6.6^{+5.0}_{-4.8} \times 10^4$ Jy sr^{-1} at 95 per cent confidence level. In this paper, we present a refinement of this earlier work by improving the mask weighting in each of the Planck bands and the precision in the covariance matrix. We report a detection of excess emission in the 545 GHz Planck band separate from the cosmic infrared background (CIB) present in the 353–857 GHz Planck bands. This excess is consistent with redshifted C II emission, in which case we report $b_{\rm C\,II} I_{\rm C\,II} = 2.0^{+1.2}_{-1.1} \times 10^5$ Jy sr^{-1} at 95 per cent confidence level, which strongly favours many *collisional excitation* models of C II emission. Our detection shows strong evidence for a model with a non-zero C II parameter, though line intensity mapping observations at high spectral resolution will be needed to confirm this result.

Key words: ISM: molecules – galaxies: high-redshift – cosmology: observations – cosmology: theory – large-scale structure of Universe – submillimetre: ISM.

1 INTRODUCTION

The star formation rate steadily increases after the first galaxies form and then dramatically declines by a factor of 20 from $z \sim 3$ to the present. One key to solve this quenching puzzle may be the interstellar medium (ISM), which provides the birthplace of stars and plays a crucial role in galaxy evolution. Studies of the molecular and fine structure lines emitted from different phases of the ISM are particularly useful to unveil the ISM properties during the epoch of interest (Carilli & Walter 2013).

C II, the fine structure line from ionized carbon, is a strong tracer of star formation. Since the ionization energy of carbon $E_{\rm C\,II} = 11.26$ eV is less than the 13.6 eV required to ionize hydrogen, ionized carbon is abundant under a wide variety of conditions. When the gas temperature is higher than 91 K, C II is excited through the $^2P_{3/2} \rightarrow {}^2P_{1/2}$ transition, which produces the C II emission line at 157.7 μm. C II is the brightest far-infrared line, contributing 0.1–1 per cent of the total far-infrared luminosity of the nuclear region of galaxies, and has been successfully detected out to redshift 7 by the Atacama Large Microwave Submillimeter Array (ALMA) (Bradač et al. 2017). However, traditional galaxy redshift surveys have limitations. First, surveys at high redshift tend only to resolve the brightest sources, resulting in a sample that is not representative of the average galaxy population (Bouwens et al. 2015). On the other hand, surveys with small area at low redshift may have high cosmic variance. Secondly, since high-flux sensitivity drives large apertures, spectroscopic surveys for individual galaxies are expensive. Instead of resolving individual objects, we pursue an emerging approach known as intensity mapping (IM). IM is a blind and unbiased measurement. It integrates the emission along the line of sight from all sources, so it can capture faint sources across large volumes and only requires modest aperture sizes. IM was originally developed to study 21 cm radiation from reionization but has been applied to mapping other bright lines (Hogan & Rees 1979; Scott & Rees 1990; Madau, Meiksin & Rees 1997; Suginohara, Suginohara & Spergel 1999; Chang et al. 2008; Wyithe, Loeb & Geil 2008; Kovetz et al. 2017).

Pullen et al. (2018), hereafter AP2018, sought to measure the intensity of C II cumulative emission through cross-correlating intensity maps with other tracers of large-scale structure (LSS). This measurement is later used in constraining the evolution of C II luminosity (Padmanabhan 2019). Although AP2018 reported a C II intensity brightness at redshift $z \sim 2.6$, Bayesian analysis did not show a strong preference for an emission model that requires C II versus one without C II. To simplify the mode-coupling matrix calculation for the angular power spectrum measurement under partial sky coverage, AP2018 used the apodized product of the Planck and galaxy surveys binary masks as a common weight for all maps. This map weighting scheme simplifies the estimator but makes it less optimal in two ways: (1) AP2018 neglect the differences of the coverage between Planck × quasar (QSO) and

★ E-mail: sy1823@nyu.edu

the Planck × CMASS luminous red galaxy (LRG) when measuring the autopower spectra of the Planck intensity maps, which are used to construct the covariance matrix, and (2) the binary mask does not reflect the variation in noise across the Planck or LSS survey.

In this letter, we follow the measurement method proposed by AP2018, but employ more optimal map weighting. We detect an anomalous intensity consistent with C II line emission at $z \sim 2.6$ with the constraint $b_{\rm C\,II} I_{\rm C\,II} = 2.0^{+1.2}_{-1.1} \times 10^5\,{\rm Jy\,sr^{-1}}$ at 95 per cent confidence level, where $b_{\rm C\,II}$ is the clustering bias of the C II emitters. Our Bayesian evidence calculation shows strong preference for C II emission in the model. We also test our measurement for systematic effects and compare it to the predictions of several promising theoretical models. However, we cannot rule out an unknown extragalactic source, which also correlates with the QSO overdensity, emitting at around 1900 GHz in the rest frame, or a cosmic infrared background (CIB) model with an erroneous redshift or spectral dependence, thus we do not claim a C II detection. If we interpret the excess as a C II detection, the *collisional excitation* models are strongly preferred.

2 DATA

Following AP2018, we cross-correlate Planck intensity maps with LSS tracer maps and perform a Monte Carlo Markov Chain (MCMC) analysis. The Planck maps we use are from the High-Frequency Instrument (HFI) in frequency channels 353, 545, and 857 GHz (Lamarre et al. 2010; Planck HFI Core Team VI 2011). Two LSS surveys we use are the Sloan Digital Sky Survey (SDSS) III (Eisenstein et al. 2011) Baryon Oscillation Spectroscopic Survey (BOSS) spectroscopic quasar sample from Data Release 12 (DR12) and the CMASS spectroscopic galaxy sample from BOSS DR12 (Dawson et al. 2013). Details about the telescope and instruments of SDSS can be found in Fukugita et al. (1996), Gunn et al. (1998, 2006), Doi et al. (2010), and Smee et al. (2013). Since the rest-frame frequency of C II is $\nu_{\rm C\,II} = 1901.3$ GHz and the redshift range of the BOSS quasars is $z \in [2, 3.2]$, C II emission only appears in one cross-correlation pair between the 545 GHz Planck map and the BOSS QSO density field. Data from the other five cross-correlation angular power spectra are used to fit for the CIB parameters.

In order to test the reliability of our correlated CIB model and gain support for the C II intensity detection, we measure the cross-power between the 545 GHz Planck map and a third LSS survey, which does not participate in the parameter fitting process. The LSS survey we use is the SDSS-IV (Blanton et al. 2017; Abolfathi et al. 2018) extended Baryon Oscillation Spectroscopic Survey (eBOSS) spectroscopic quasar sample (Dawson et al. 2016).

We multiply the Planck Galactic emission mask with the combined Planck point source mask to get the base Planck mask W. To assign pixels that better reflect the Planck survey depth, we modify the base Planck mask in each frequency band as $W_i = W(\frac{1}{\langle H_i \rangle} + \frac{1}{H_i})^{-1}$, here $i = 353, 545, 857$ specify the frequency, and H_i is the hits counting map for the corresponding frequency channel. Instead of using the hits maps directly as weights, this harmonic mean form of weighting trades some optimality for keeping the mode–mode coupling manageable.

3 METHOD

The method we use to measure the angular power spectra and to compute the covariance matrix follows from AP2018. We therefore refer the reader to AP2018 for details. As a brief review, we use the pseudo-C_ℓ estimator to measure the angular power spectra from the masked maps. Unlike in AP2018, the Planck masks we use are weighted by the hits maps, as introduced in Section 2. We use the six measured cross-power spectra between Planck intensity maps and LSS maps $C_\ell^{\{353,545,857\}\times\{\rm QSO,LRG\}}$ as data in the likelihood. We also measure the autocorrelations to construct the covariance matrix. Following Hivon et al. (2002), we compute the mode–mode coupling matrices $M_{\ell\ell'}$ for all the possible mask pair combinations, which are important for an accurate covariance matrix calculation. This step is the most consequential change compared to AP2018.

We consider the multipole range $100 \leq \ell \leq 1000$ and equally bin the measurement into nine bins, each with bin width $\Delta b = 100$. We bin the mode–mode coupling matrices and the measured angular power spectra, then use the measured angular power spectra to interpolate the continuous C_ℓ and analytically compute the covariance matrix following Tristram et al. (2005). To ensure that the covariance matrix is symmetric, we follow the treatment suggested by Brown, Castro & Taylor (2005), shown in equation (11) of AP2018.

4 RESULTS

Using the measured angular power spectra and the inverse covariance matrix as inputs, we perform an MCMC exploration on the model introduced in AP2018 section 5.1. We vary the six parameters $\{L_0,\ \delta,\ T_{\rm dust},\ A_{\rm tSZ},\ A_{\rm exc},\ b_{\rm QSO}\}$, that float freely during the fitting process. We introduce these parameters below.

The angular cross-power spectrum between Planck IM and LSS tracer map $C_\ell^{\rm T-LSS}$ is modelled as equation (12) of AP2018. The clustering bias for BOSS QSO sample $b_{\rm QSO}$ is a free parameter floating in the range 3.2–3.8 (Pullen et al. 2018) in the model. We use CAMB (Lewis, Challinor & Lasenby 2000) to compute the dark matter power spectrum in this work. For the Planck CIB source, the clustering bias $b_{\rm CIB}(k, z)$ and redshift distribution ${\rm d}S/{\rm d}z$ are all predicted using the halo model introduced by Shang et al. (2012), shown in equations (13) and (14) of AP2018. The luminosity amplitude parameter L_0, redshift evolution parameter δ, and dust temperature averaged over the redshift range $T_{\rm dust}$ are all introduced to describe the galaxy luminosity $L_{\nu(1+z)}$. The galaxy spectral energy distribution (SED) $\Theta(\nu)$, which is the frequency factor in $L_{\nu(1+z)}$, is modified as $\Theta(\nu)(1 + A_{\rm exc}\delta(\nu - \nu_{\rm C\,II}))$ to account for the excess of the angular cross-power spectrum due to the C II emission. Notice that we define $C_\ell^{\rm C\,II-LSS} \propto b_{\rm CIB} A_{\rm exc} = b_{\rm C\,II}(\frac{b_{\rm CIB}}{b_{\rm C\,II}} A_{\rm exc}) = b_{\rm C\,II} A_{\rm C\,II}$ in the model, and the intensity I is proportional to the amplitude parameter A, the intensity of C II emission $I_{\rm C\,II} = \frac{b_{\rm CIB}}{b_{\rm C\,II}} I_{\rm exc}$. Assuming the clustering bias of the CIB and C II sources are identical, $I_{\rm C\,II} = I_{\rm exc}$. Finally, an amplitude parameter $A_{\rm tSZ}$ describes the contribution of correlated thermal Sunyaev–Zeldovich (tSZ) emission (Sunyaev & Zeldovich 1972), at 353 GHz.

We perform the MCMC exploration of the parameter space with a modified version of COSMOMC (Lewis & Bridle 2002). The reduced χ^2 for our fitting is $\chi^2/N_{\rm d.o.f.} = \chi^2/61 = 1.6$, while if we remove $A_{\rm C\,II}$ from the model, i.e. the $A_{\rm C\,II}$ parameter is fixed to zero, the reduced χ^2 increases to 1.9. We show the posterior of parameter $A_{\rm exc}$ in Fig. 1. The model constrains $A_{\rm exc} = 0.59^{+0.37}_{-0.33}$ at a 95 per cent confidence level, and a C II line intensity $b_{\rm C\,II} I_{\rm C\,II} = 2.0^{+1.2}_{-1.1} \times 10^5\,{\rm Jy\,sr^{-1}}$. If we assume $b_{\rm C\,II} = b_{\rm CIB}$, which we set to 2.92 according to model introduced by Tinker et al. (2010) at $z = 2.6$, we find $I_{\rm C\,II} = 6.9^{+4.2}_{-3.8} \times 10^4\,{\rm Jy\,sr^{-1}}$, consistent with the value from AP2018 but with lower uncertainty. The best-fitting values for other parameters are $L_0 = 0.245^{+0.040}_{-0.036}$, $\delta = 2.37^{+0.19}_{-0.21}$, $T_{\rm dust} = 28.3^{+1.3}_{-1.4}$ K, $A_{\rm tSZ} = 0.78^{+0.44}_{-0.47}$, and $b_{\rm QSO} = 3.32^{+0.32}_{-0.13}$ at 95 per cent confidence level.

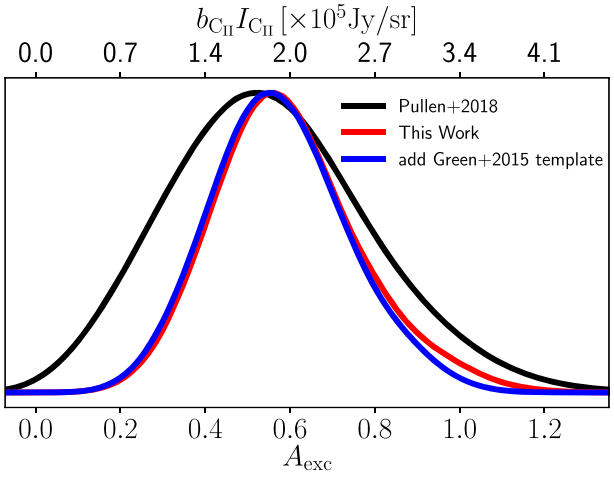

Figure 1. Posterior of the C II emission line intensity parameter $A_{\rm exc}$ from MCMC.

The three other parameters used in the theoretical $C_\ell^{\rm T-LSS}$ model: β introduced as the emissivity in the SED, and $M_{\rm eff}$, $\sigma^2_{L/m}$ used in the lognormal dark matter halo mass dependence of the galaxy luminosity have descending impact on the $C_\ell^{\rm T-LSS}$. Following AP2018, we fix these three parameters as: $\log_{10}(M_{\rm eff})[{\rm M}_\odot] = 12.6$, $\sigma^2_{L/m} = 0.5$, and $\beta = 1.5$, but even if we let β or $M_{\rm eff}$ float in the MCMC process, the fitting result for $A_{\rm exc}$ is almost unchanged. We perform several tests for robustness of the detection to uncertainties in the model. The following variations produce slight shifts in the posterior distribution of $A_{\rm exc}$, but a negligible impact on the detection significance: (1) a 10 per cent uncertainty in $b_{\rm CIB}$ (van Engelen et al. 2015), (2) an alternate (broader) prior on $b_{\rm QSO}$ between 3.6 and 4.3 (White et al. 2012), (3) a shift to $M_{\rm min}$ under 10^{11} M$_\odot$.

Our fitting results differ from AP2018 mainly because AP2018 use the product of the Planck mask and the galaxy survey mask as the final mask to compute $\hat{C}_b^{\rm TL}$. When computing $Cov[\hat{C}_b^{\rm T\times QSO}, \hat{C}_{b'}^{\rm T\times LRG}]$, which requires the autocorrelation of Planck maps, AP2018 assume that CMASS galaxy mask and BOSS QSOs mask are similar and use the product of the Planck mask and BOSS QSOs mask to measure $C_\ell^{\rm TT}$ for simplicity. Since the mode–mode coupling matrices are computationally expensive, this approach is faster but reduces optimality of the estimator. In this work, we distinguish the weight for each map and compute all the mode–mode coupling matrices that are needed to keep the covariance matrix as accurate as possible. As a result, the $A_{\rm exc}$ measurement does not shift much, but the standard deviation in this work decreases by a factor of 1.4.

5 TESTS OF DETECTION

5.1 Bayesian analysis

To test if this non-zero excess emission is a true detection, we use Bayesian evidence with the Laplace approximation (Heavens 2009) to determine if introducing the parameter $A_{\rm exc}$ into the model is preferred. We find the Bayesian evidence $\langle B\rangle = 0.066$, which shows a strong preference to the model with a free $A_{\rm exc}$ parameter.

Following Switzer et al. (2019), hereafter S2019, which consider the cross-power with the Green et al. (2015) Milky Way template to provide additional leverage to suppress foregrounds, we add a term to the model which can accommodate correlations between the Green et al. (2015) model and LSS due to systematics. This is parametrized as amplitude α times the CIB clustering anisotropy template. COSMOMC fits (Fig. 1) $A_{\rm exc} = 0.57^{+0.33}_{-0.31}$ under S2019 model, corresponding to a mean intensity of $b_{\rm C\,II} I_{\rm C\,II} = 2.0^{+1.0}_{-1.1} \times 10^5$ Jy sr^{-1} (95 per cent confidence level). The Bayesian evidence between the S2019 models with/without $A_{\rm exc}$ parameter is $\langle B\rangle = 0.030$, which shows an even stronger preference to C II emission line detection. We then compare the AP2018 model with the S2018 model, both with a free $A_{\rm exc}$ parameter, but the S2019 model contains an extra parameter α. We get $\langle B\rangle = 11.29$, showing a strong preference to the AP2018 model. This indicates that with current data, projecting out foregrounds using the Green et al. (2015) template is not enough to compensate the overfitting effect caused by introducing an extra parameter. We therefore report the fitting result $b_{\rm C\,II} I_{\rm C\,II} = 2.0^{+1.2}_{-1.1} \times 10^5$ Jy sr^{-1} and $I_{\rm C\,II} = 6.9^{+4.2}_{-3.8} \times 10^4$ Jy sr^{-1} as our final conclusion in this work.

Table 1. Fractional contribution by interloping spectral lines in Planck-LSS and CII-QSO angular power spectra. The deviation is small compared to error in this work.

C_ℓ	Interloper	$\Delta C_\ell/C_\ell$[%]
353-QSO	^{12}CO(10-9),^{12}CO(11-10), ^{12}CO(12-11)	0.69
545-QSO	O I	0.34
857-QSO	O III	1.3
353-CMASS	^{12}CO(5-4),^{13}CO(5-4),HCN(6-5)	2.5
545-CMASS	^{12}CO(7-6),^{12}CO(8-7),CI, ^{13}CO(7-6),^{13}CO(8-7)	1.5
857-CMASS	^{12}CO(11-10),^{12}CO(12-11),N II	0.55
C II-QSO	all interlopers	2.5

5.2 Statistical tests

Spectral line contamination can bias the measurement. Besides C II, other fine-structure emission lines such as O I (145 μm), O III (88 μm), and N II(205 μm) will contribute to the six sets of angular power spectra. To test how much the contamination from other lines influences the data, we include lines from table 1 of Visbal & Loeb (2010) and theoretically compute the fractional deviation of angular power spectra compared to the original $C_\ell^{\rm TL}$s under the best-fitting parameters. The results are summarized in Table 1. $C_\ell^{\rm CII-QSO}$ only increases by 2.5 per cent, and all $C_\ell^{\rm T-LSS}$ involved in the theoretical model increase less than 3 per cent. Since the measurement error of $\hat{C}_\ell$ is larger than 13 per cent, deviation to $A_{\rm exc}$ caused by interloper lines are not significant in this work. For interlopers to matter at the 1σ level, the ratio of C II to interloper lines based on Visbal & Loeb (2010) would need to be overestimated by a factor of five.

The continuum foreground contamination from the Milky Way, which is not statistically isotropic, is another concern for IM measurements. The LSS tracer maps we use themselves would not have MW emission, but the selection function may be impacted by bright galactic emission. To test if the measured angular power spectra converge under decreasing survey area, we replace the 40 per cent Planck Galactic emission mask with a 20 per cent mask and redo the angular power spectra measurement. The difference between the original measurement and the measurement under the smaller area is well within the uncertainty. Additionally, we divide the Planck and QSO (LRG) surveys into 47 (42) and find that the Jackknife over these regions is consistent with reported errors. The distribution of the cross-correlation between Gaussian signal simulations and the Planck map is consistent with the standard deviation of the simulations, which indicates that the non-Gaussian

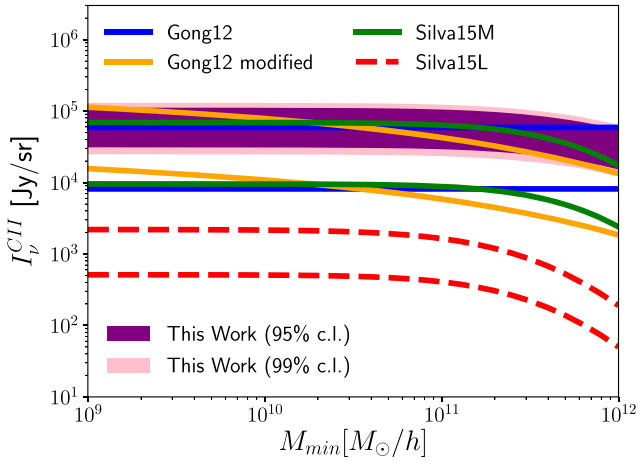

Figure 2. C II intensity measurement in this work at 95 per cent and 99 per cent confidence level and the theoretical predictions from Gong et al. (2012), Silva et al. (2015), and Pullen et al. (2018) .

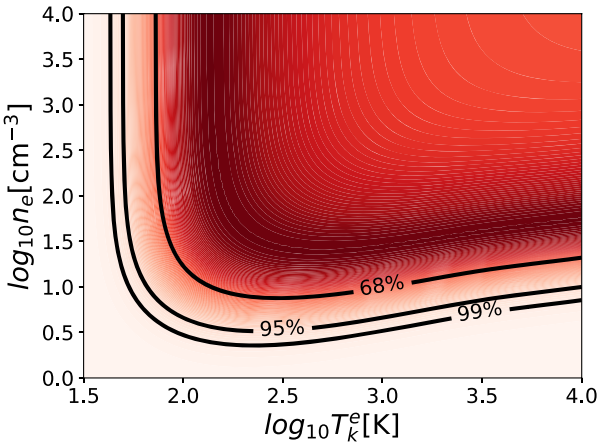

Figure 3. Contours of posterior $p[I_{\rm C\,II}(T_{\rm k}^{\rm e}, n_{\rm e})]$ at 68 per cent, 95 per cent, and 99 per cent confidence levels. The intensity of C II line $I_{\rm C II}$ at redshift $z = 2.6$ is theoretically computed from 'Gong12 modified' model. The darker region is in the higher confidence level.

contribution to the error from diffuse Milky Way emission is negligible.

5.3 Tests of the correlated CIB model

A systematic error in the CIB model could be attributed incorrectly to C II emission and still produce an overall reasonable χ^2 value. To test if the best-fitting CIB model is accurate, we use the best-fitting CIB parameters $\{L_0, \delta, T_{\rm dust}\}$ to predict the angular cross-power spectra between Planck CIB maps in 353, 545, 857 GHz frequency channel and the eBOSS QSO map. We then compare the theoretical prediction with measurement through a χ^2 test. We use the clustering bias fitted by Laurent et al. (2017) for eBOSS QSO. The theoretically estimated angular cross-power spectra agree with the measurements. The reduced $\chi^2 = 1.22$, 1.54, 1.62 for $C_\ell^{353\times\rm eBOSSQSO}$, $C_\ell^{545\times\rm eBOSSQSO}$, and $C_\ell^{857\times\rm eBOSSQSO}$, respectively.

We further perform an MCMC on the best-fitting CIB parameters. We introduce another free parameter $A_{\rm null}$ and assume $[C_\ell^{545\times\rm eBOSSQSO}]_{\rm data} = (1 + A_{\rm null}) \times [C_\ell^{545\times\rm eBOSSQSO}]_{\rm camb}$ in the theoretical model, where $[C_\ell]_{\rm data}$ is the measured angular power spectrum, while $[C_\ell]_{\rm camb}$ is theoretically computed through equation (12) of AP2018 based on the best-fitting CIB parameters. We set a constant prior of $A_{\rm null}$ from -1 to 1 and fit for the seven free parameters through COSMOMC. We get $A_{\rm null} = 0.04^{+0.18}_{-0.18}$ at 95 per cent confidence level while other CIB/C II parameters do not change significantly. Hence, these additional cross-correlation channels are fully consistent with the correlated CIB model, and do not show any excess analogous to 545 GHz cross quasars. Since $C_\ell^{\rm CIB\times eBOSSQSO}$ is not involved in the parameter fitting process, this result brings extra support to the reliability to the CIB model.

5.4 Constraints on theoretical models

If we interpret the excess correlated emission of Planck 545 GHz cross quasars as C II, we can make additional statements about the excitation of the gas. Fig. 2 shows the C II constraint consistent with our excess measurement (assuming $b_{\rm CIB} = b_{\rm C\,II}$) together with the theoretical predictions from models Gong et al. (2012) (Gong12), Silva et al. (2015) (Silva15), and the modified Gong12 model introduced by AP2018. We include the impact of $M_{\rm min}$ on $b_{\rm CIB}(M)$ and $n(M)$, which is the number density of haloes with mass above M. As M increases, $b_{\rm CIB}(M)$ rises and $n(M)$ falls. Since $C_\ell^{\rm C\,II\text{-}QSO} \sim I_{\rm C\,II} b_{\rm CIB}$ and $I_{\rm C\,II} \propto n(M)$, increase in $M_{\rm min}$ results in a decline of $I_{\rm C\,II}$. 'Gong12', 'Gong12 modified', and 'Silva15M' are *collisional excitation* models, in which the C II intensity is derived through solving the statistical balance equation between the upper level $^2P_{3/2}$ and the lower level $^2P_{1/2}$ of C II fine structure line. The upper bound of Fig. 2 corresponds to an infinite spin temperature for the C II transition while the lower bound corresponds to kinetic temperature of the electron $T_{\rm k}^{\rm e} = 100$ K and the number density of electron $n_{\rm e} = 1\,{\rm cm}^{-3}$. 'Silva15L' belongs to *scaling relations* models, in which C II intensity is modelled based on measured luminosity function. The upper/lower bound is model 'm1'/'m4' in Silva et al. (2015) table 1. We find our measurement favours *collisional excitation* models. 'Silva15L' is lower than the lower limit of our measurement at 99 per cent confidence level, thus the *scaling relations* models such as 'Silva15L' are strongly disfavoured by our measurement. However, our 'Silva15L' model is extrapolated from redshift $z = 6$, so we do not completely rule it out.

In addition, assuming an excess modelled as a C II intensity can constrain the kinetic temperature of the electron $T_{\rm k}^{\rm e}$ and number density of electron $n_{\rm e}$ in the theoretical model 'Gong12 modified'. The contour of the $I_{\rm C\,II}$ posterior is shown in Fig. 3. The upper bound of 'Gong12 modified' shown in Fig. 2 corresponds to $T_{\rm k}^{\rm e} \to \infty$ and $n_{\rm e} \to \infty$ in the parameter space, which is within 95 per cent confidence level of our measurement. Fig. 3 also shows the asymptotic behaviour of $I_{\rm C\,II}(T_{\rm k}^{\rm e}, n_{\rm e})$ at very high kinetic temperature or electron number density. Another observable is needed to break the degeneracy between $T_{\rm k}^{\rm e}$ and $n_{\rm e}$. One possibility would be another fine structure line which also depends on ionization of the ISM. Another is a measurement of the one-point PDF of C II intensities (Breysse et al. 2017; Ihle et al. 2019) which samples the full luminosity function instead of just the first moment like the intensity.

6 CONCLUSIONS

This work is the most significant detection of an excess consistent with the C II emission line from intensity maps. We use the model proposed by AP2018: using the angular cross-power spectra between Planck intensity maps in frequency 353, 545, 857 GHz and both BOSS quasars and CMASS galaxies to constrain a source

of emission correlated with LSS consistent with C II emission at redshift $z \sim 2.6$ with $b_{\rm C\,II} I_{\rm C\,II} = 2.0^{+1.2}_{-1.1} \times 10^5$ Jy sr^{-1} at 95 per cent confidence level, which is strongly preferred as Bayesian evidence. We find contamination from foreground anisotropy and interloper lines are not significant compared to measurement error for the data we use. Our best-fitting CIB model can also successfully predict the angular cross-power spectrum between Planck intensity maps and eBOSS quasars, supporting the reliability of our fitting results. Among the C II models considered in this work, the C II constraint favours many *collisional excitation* models. We study the posterior of C II line intensity as a function of electron kinetic temperature $T_{\rm k}^{\rm e}$ and number density $n_{\rm e}$ under the theoretical model introduced by Gong et al. (2012) and AP2018. Based on the C II intensity constraint consistent with this work, we can constrain the values of $T_{\rm k}^{\rm e}$ and $n_{\rm e}$. $T_{\rm k}^{\rm e}$ and $n_{\rm e}$ are degenerate in the modified Gong et al. (2012) model. Measurements of other observables such as the intensity or luminosity functions of other fine structure lines may be able to break the $T_{\rm k}^{\rm e}$-$n_{\rm e}$ degeneracy.

In this paper we refrain from claiming that the excess we measure is a confident detection of C II, considering we cannot rule out that our excess is due to redshift evolution of the CIB parameters, in particular the spectral index β. The resolution to this question will require upcoming line IM surveys which will be able to use high spectral resolution to discriminate between C II line emission and continuum CIB emission.

ACKNOWLEDGEMENTS

We would thank Shenglong Wang for the IT support. We also thank Michael Blanton, Jeremy Tinker, Patrick Breysse, and Dou Liu for useful discussions.

This work is based on observations obtained with *Planck* (http://www.esa.int/Planck), an ESA science mission with instruments and contributions directly funded by ESA Member States, NASA, and Canada.

Funding for SDSS-III and IV have been provided by the Alfred P. Sloan Foundation, the Participating Institutions, the National Science Foundation, and the U.S. Department of Energy Office of Science. SDSS-IV acknowledges support and resources from the Center for High-Performance Computing at the University of Utah. The SDSS web site is www.sdss.org.

SDSS-III and IV are managed by the Astrophysical Research Consortium for the Participating Institutions of the SDSS Collaboration including the University of Arizona, the Brazilian Participation Group, Brookhaven National Laboratory, the Carnegie Institution for Science, Carnegie Mellon University, the Chilean Participation Group, University of Florida, the French Participation Group, the German Participation Group, Harvard University, Instituto de Astrofísica de Canarias, the Michigan State/Notre Dame/JINA Participation Group, Johns Hopkins University, Kavli Institute for the Physics and Mathematics of the Universe (IPMU) / University of Tokyo, the Korean Participation Group, Lawrence Berkeley National Laboratory, Leibniz Institut für Astrophysik Potsdam (AIP), Max-Planck-Institut für Astronomie (MPIA Heidelberg), Max-Planck-Institut für Astrophysik (MPA Garching), Max-Planck-Institut für Extraterrestrische Physik (MPE), National Astronomical Observatories of China, New Mexico State University, New York University, University of Notre Dame, Observatário Nacional / MCTI, Ohio State University, Pennsylvania State University, Shanghai Astronomical Observatory, United Kingdom Participation Group, Universidad Nacional Autónoma de México, University of Arizona, University of Colorado Boulder, University of Oxford, University of Portsmouth, Princeton University, the Spanish Participation Group, University of Utah, Vanderbilt University, University of Virginia, University of Washington, University of Wisconsin, Vanderbilt University, and Yale University.

REFERENCES

Abolfathi B. et al., 2018, ApJS, 235, 42
Blanton M. R. et al., 2017, AJ, 154, 28
Bouwens R. J. et al., 2015, ApJ, 803, 34
Bradač M. et al., 2017, ApJ, 836, L2
Breysse P. C., Kovetz E. D., Behroozi P. S., Dai L., Kamionkowski M., 2017, MNRAS, 467, 2996
Brown M. L., Castro P. G., Taylor A. N., 2005, MNRAS, 360, 1262
Carilli C. L., Walter F., 2013, ARA&A, 51, 105
Chang T.-C., Pen U.-L., Peterson J. B., McDonald P., 2008, Phys. Rev. Lett., 100, 091303
Dawson K. S. et al., 2013, AJ, 145, 10
Dawson K. S. et al., 2016, AJ, 151, 44
Doi M. et al., 2010, AJ, 139, 1628
Eisenstein D. J. et al., 2011, AJ, 142, 72
Fukugita M., Ichikawa T., Gunn J. E., Doi M., Shimasaku K., Schneider D. P., 1996, AJ, 111, 1748
Gong Y., Cooray A., Silva M., Santos M. G., Bock J., Bradford C. M., Zemcov M., 2012, ApJ, 745, 49
Green G. M. et al., 2015, ApJ, 810, 25
Gunn J. E. et al., 1998, AJ, 116, 3040
Gunn J. E. et al., 2006, AJ, 131, 2332
Heavens A., 2009, preprint (arXiv:0906.0664)
Hivon E., Górski K. M., Netterfield C. B., Crill B. P., Prunet S., Hansen F., 2002, ApJ, 567, 2
Hogan C. J., Rees M. J., 1979, MNRAS, 188, 791
Ihle H. T. et al., 2019, ApJ, 871, 75
Kovetz E. D. et al., 2017, preprint (arXiv:1709.09066)
Lamarre J.-M. et al., 2010, A&A, 520, A9
Laurent P. et al., 2017, J. Cosmol. Astropart. Phys., 7, 017
Lewis A., Bridle S., 2002, Phys. Rev. D, 66, 103511
Lewis A., Challinor A., Lasenby A., 2000, ApJ, 538, 473
Madau P., Meiksin A., Rees M. J., 1997, ApJ, 475, 429
Padmanabhan H., 2019, MNRAS, 488, 3
Planck HFI Core Team VI, 2011, A&A, 536, A6
Pullen A. R., Serra P., Chang T.-C., Doré O., Ho S., 2018, MNRAS, 478, 1911
Scott D., Rees M. J., 1990, MNRAS, 247, 510
Shang C., Haiman Z., Knox L., Oh S. P., 2012, MNRAS, 421, 2832
Silva M., Santos M. G., Cooray A., Gong Y., 2015, ApJ, 806, 209
Smee S. A. et al., 2013, AJ, 146, 32
Suginohara M., Suginohara T., Spergel D. N., 1999, ApJ, 512, 547
Sunyaev R. A., Zeldovich Y. B., 1972, Comments Astrophys. Space Phys., 4, 173
Switzer E. R., Anderson C. J., Pullen A. R., Yang S., 2019, ApJ, 872, 82
Tinker J. L., Robertson B. E., Kravtsov A. V., Klypin A., Warren M. S., Yepes G., Gottlöber S., 2010, ApJ, 724, 878
Tristram M., Macías-Pérez J. F., Renault C., Santos D., 2005, MNRAS, 358, 833
van Engelen A. et al., 2015, ApJ, 808, 7
Visbal E., Loeb A., 2010, J. Cosmol. Astropart. Phys., 11, 016
White M. et al., 2012, MNRAS, 424, 933
Wyithe J. S. B., Loeb A., Geil P. M., 2008, MNRAS, 383, 1195

This paper has been typeset from a TEX/LATEX file prepared by the author.